DOI: 10.1002/ ((please add manuscript number))
Article type: Full Paper

Enhancing the Efficiency of Organic Photovoltaics by a Photoactive Molecular Mediator

Bin Yang, Matthew A. Kolaczkowski, Michael A. Brady, Jong K. Keum, James F. Browning, Teresa L. Chen, Yi Liu*

Dr. Bin Yang, Matthew A. Kolaczkowski, Dr. Michael A. Brady, Teresa L. Chen, Dr. Yi Liu
The Molecular Foundry, Lawrence Berkeley National Laboratory, Berkeley, California 94720, United States
Email: yliu@lbl.gov
Dr. Bin Yang
College of Materials Science and Engineering, Key Laboratory for Micro-Nano Physics and Technology of Hunan Province, Hunan University, Changsha, Hunan 410082, P. R. China
Dr. Michael A. Brady
Advanced Light Source, Lawrence Berkeley National Laboratory, Berkeley, California 94720, United States
Dr. Jong K. Keum, Dr. James F. Browning
Center for Nanophase Materials Sciences, Oak Ridge National Laboratory, Oak Ridge, Tennessee 37831, United States
Dr. Jong K. Keum
Chemical and Engineering Materials Division, Oak Ridge National Laboratory, Oak Ridge, Tennessee 37831, United States

Keywords: Conjugated molecular materials; Organic optoelectronics; Organic photovoltaics; Morphology

Abstract: High boiling-point solvent additives, such as 1,8-diiodooctane, have been widely used to tune nanoscale phase morphology for increased efficiency in bulk heterojunction organic solar cells. However, liquid-state solvent additives remain in the active films for extended times and later migrate or evaporate from the films, leading to

unstable device performance. Here, we report a solid-state photoactive molecular mediator, namely $N(BAI)_3$, that could be employed to replace the commonly used solvent additives to tune the morphology of bulk heterojunction films for improved device performance. The $N(BAI)_3$ mediator not only resides in the active films locally to fine tune the phase morphology, but also contributes to the additional absorption of the active films, leading to ~ 11% enhancement of power conversion efficiency of P3HT:$PC_{60}BM$ devices. Comparative studies were carried out to probe the nanoscale morphologies using grazing incidence wide-angle X-ray scattering and complementary neutron reflectometry. The use of 1 wt% $N(BAI)_3$ was found to effectively tune the packing of P3HT, presumably through balanced π-interactions endowed by its large conjugated π surface, and promote the formation of a $PC_{60}BM$-rich top interfacial layer. These findings open up a new way to effectively tailor the phase morphology by photoactive molecular mediators in organic photovoltaics.

1. Introduction

Solution-processed organic photovoltaics (OPVs) have drawn increasing attention in the past few decades[1, 2] for their potential use as building-integrated photovoltaics, which is attractive not only for providing a viable renewable energy solution, but also for meeting the artistic needs of building design using organic materials with tunable optical properties.[1, 3, 4] Such applications, however, are still limited by the inferior device stability and low power conversion efficiency (PCE) of OPVs. Recently, the PCE in single junction OPVs has been raised to ~13% through design and synthesis of new

photoactive organic materials (e.g. low bandgap non-fullerene acceptors).[5] Further improvement in both device stability and PCE requires the tuning of supramolecular organization (e.g. molecular packing, molecular orientation) and nanoscale phase morphology (e.g. domain size, donor/acceptor phase separation).[6] Ideally, the domain size of the donors and acceptors should be smaller than the exciton diffusion length, typically less than 20 nm,[4] to ensure successful exciton dissociation. At the same time, the donor and acceptor domains should form inter-domain percolation pathways to ensure efficient charge transport and collection. Previous studies have shown that the bulk heterojunction morphology can be tailored by a trace amount of high boiling-point solvent processing additives, such as 1,8-diiodooctane (DIO)[7] and chloronaphthalene (CN),[8] to improve the nanoscale phase separation and intercalation between polymer donors and fullerene acceptors for enhanced PCEs.[9, 10] However, solvent additives[11, 12, 13] remain in the active films for extended times, leading to unstable device performance.[11, 13] It was found that the devices with DIO degraded faster than those without DIO due to the faster evolution of nanophase morphology during the slow evaporation or migration of solvent additive residues in the bulk heterojunction films.[10, 11] An alternative approach is to introduce solid state molecular mediators which will remain in the thin film while tuning the phase morphology. This approach has been demonstrated in both organic field effect transistors[14] and OPVs,[15] in which a small amount of "impurities" were blended with the matrix of organic semiconductors to impose supramolecular ordering on the matrix molecules by noncovalent intermolecular interactions.[14] In addition to morphology tuning, molecular mediators for OPVs can

further enhance device performances by more effective absorption of sunlight. This aspect, however, has remained rarely explored in OPVs.

Triphenylamines (TPA) provide a scaffold to address this problem, and have seen consistent use as a motif in a variety of organic electronics applications, primarily as donor materials due to high HOMO levels.[16] Conjugation with electron withdrawing groups such as diketopyrrolopyrrole (DPP) has allowed TPA to find use as acceptor and ambipolar materials as well.[17] These donor-acceptor type triphenylamines have high extinction coefficients where the HOMO-LUMO gap can be modified by the strength of the pendant withdrawing groups.

Another interesting feature of TPA is the ability to self-assemble, often stacking face-to-face to form nanowires. Both photo and chemical oxidation of TPA to the radical cation have been shown to facilitate this interaction, where charge can be stabilized through delocalization throughout the wire stack.[18] Additional aggregate stability can be provided through the aromatic π–π interactions with neighboring molecules. Such highly favorable intramolecular and electronic interactions of TPA could be harnessed to interact with other molecules or polymers in order to benefit both phase morphology and electronic properties of the parent system.

Based on the above mentioned concept, we have recently developed a series of bay-annulated indigo (BAI) based donor-acceptor materials,[19-21] including the trimeric $N(BAI)_3$ (Figure 1) with a TPA core unit and three pendent BAI acceptor units.[20] Such class of materials have extended π conjugation surface, good solution processability,

strong electron accepting ability, low optical bandgap (~1.5 eV), excellent charge transport and photoresponse properties that are critical for high performance organic thin film transistors (OTFTs) and other optoelectronic devices.[19] It is conceived that the intriguing structural features of $N(BAI)_3$ will impact the nanophase separation in the active layer of OPVs, however such effect has never been demonstrated before. In this work, we demonstrate that $N(BAI)_3$ could not only be used as a solid-state molecular mediator to effectively tune the packing of active materials in poly(3-hexylthiophene-2,5-diyl) (P3HT):$PC_{60}BM$ based bulk heterojunction OPV devices, but also contribute to additional absorption of the (P3HT):$PC_{60}BM$ active films, resulting in ~11% enhancement of device efficiency. This solid-state photoactive molecular mediator can be employed as an alternative to the commonly used solvent additives for improved film morphology and optical absorption and device performance.

2. Results and Discussion

Grazing incidence wide angle X-ray scattering (GIWAXS) was employed to characterize the pure as-cast $N(BAI)_3$ film and to understand the molecular packing and orientation with respect to the substrate. As shown in the inset of **Figure S1**, strong X-ray scattering arcs were observed along both out-of-plane and in-plane directions for the as-cast film of $N(BAI)_3$, indicating good crystallinity and a preferred edge-on orientation of the π-stacked $N(BAI)_3$ molecules. Top-contact bottom-gate thin film transistor devices were fabricated to check the charge transport properties of the as-cast $N(BAI)_3$ film. The device showed p-type behavior and an average hole mobility of $\sim 9\times10^{-5}$ $cm^2V^{-1}s^{-1}$ (**Figure S1**), which is comparable to common p-type organic photovoltaic materials.[22]

To assess how $N(BAI)_3$ tunes the molecular packing and nanoscale morphology as well as photovoltaic performance, a P3HT:$PC_{60}BM$ model system was selected, to which $N(BAI)_3$ was added. **Figure 1a** shows the typical device structure (ITO/PEDOT:PSS/P3HT:$PC_{60}BM$:$N(BAI)_3$/Ca/Al) and molecular structures of the three components in the active layer. The energy diagram of the ternary devices (**Figure 1b**) shows that the energy levels of $N(BAI)_3$ align well with these of P3HT and $PC_{60}BM$. Such an energy level cascade allows for efficient photoinduced charge separation within the three-component bulk active layer.

We firstly characterized the variation of photovoltaic performance when tuning the composition ratio of $N(BAI)_3$ in the P3HT:$PC_{60}BM$ mixture films. The P3HT:$PC_{60}BM$ control device containing no $N(BAI)_3$ exhibited an open-circuit-voltage (V_{OC}) of 0.595 V, a short-circuit-current-density (J_{SC}) of 9.2 mA/cm^2, a fill-factor (*FF*) of 67% and a PCE of 3.7% (**Figure 1c**), which are consistent with the performance of typical P3HT:$PC_{60}BM$ devices.[2, 23] A 11% enhancement of PCE was realized by adding only 1 wt% $N(BAI)_3$ mediator into the P3HT:$PC_{60}BM$ blend film, together with the following device characteristics: V_{OC} 0.585 V, J_{SC} 10.0 mA/cm^2, *FF* 70% and PCE 4.1%. Adding more $N(BAI)_3$ mediator, for example 5 wt% and 10 wt%, however, resulted in a dramatic decrease in the PCE to 2.5% and 0.5%, respectively. The decrease of PCEs is mainly correlated to the variation in J_{SC} upon increasing the percentage of $N(BAI)_3$ mediator.

To verify the $N(BAI)_3$ induced variation in J_{SC}, the external quantum efficiencies (EQEs) of the devices were measured (**Figure 2a**). Compared to the $N(BAI)_3$-free devices, the EQEs in the spectral range 450-680 nm increased when adding 1 wt% $N(BAI)_3$ into the P3HT:$PC_{60}BM$ blend film, whereas the introduction of more $N(BAI)_3$

mediator led to the decrease in EQE in this region, which was consistent with the variation trend in J_{SC}. Concomitantly, the EQE between 680 nm and 870 nm was enhanced for thin films employing $N(BAI)_3$ up to 5 wt%, suggesting the small but positive contribution to J_{SC} from the lower energy optical absorption of $N(BAI)_3$. This low energy contribution from $N(BAI)_3$ is supported by the facts that 1) negligible EQEs in the spectral range 680- 870 nm were observed for the $N(BAI)_3$-free devices, and 2) the increase in the compositional ratio of $N(BAI)_3$ led to EQE enhancement in the same spectral range. Normalization of the EQE curves revealed that the EQEs from 680 nm to 870 nm increased monotonically with rising $N(BAI)_3$ percentage (inset in **Figure 2a**), further confirming the $N(BAI)_3$'s contribution to the photocurrent generation.

The above device study has shown that the photovoltaic performance is sensitive to the loading amount of $N(BAI)_3$ in the P3HT:$PC_{60}BM$ blend films. As revealed by the analysis of the dark currents of the relative devices (**Figure S2**), adding only 1 wt% $N(BAI)_3$ resulted in the decrease in series resistance and increase in shunt resistance, whereas further introduction of $N(BAI)_3$ led to the increase in series resistance and decrease in shunt resistance (**Table S1**). Such variation of parasitic electrical characteristics suggests that the variation of device performance is likely due to morphological changes in the active layer induced by the introduction of $N(BAI)_3$ mediators.

UV-vis spectroscopic studies were carried out on the P3HT-only film and P3HT films blended with different $N(BAI)_3$ ratio to probe the polymer-$N(BAI)_3$ interactions. As shown in **Figure 2b**, three characteristic peaks (510 nm, 550 nm, and 600 nm) are assigned to 0-2, 0-1, and 0-0 vibronic transitions from the ground state to excited states

(**Figure S3**).[24, 25] By comparing the ratio of peak intensity among 0-2, 0-1, and 0-0 transitions, we found that the intensity of 0-0 transition was slightly enhanced by adding only 1 wt% $N(BAI)_3$ (**Table S2**), indicating that $N(BAI)_3$ can enhance inter-chain π-π stacking of P3HT, while adding more $N(BAI)_3$ decreased the π-π stacking of P3HT.[24] The variation of photoluminescence (PL) spectra of these films was also studied. As shown in **Figure S4**, the (0-0) vibronic transition at 670 nm was enhanced upon adding 1 wt% $N(BAI)_3$, as a result of the enhanced π-π stacking of P3HT molecules, whereas adding more $N(BAI)_3$ (10 wt%) decreased the (0-0) transition peak, which was consistent with the observation from the absorption spectra study. Atomic force microscopy (AFM) was further utilized to gain insight into the phase segregation behavior. The contrast in the AFM phase image of P3HT and $PC_{60}BM$-rich domains arises due to differences in elasticity and phase angle change response of the cantilever.[26] Compared to the pristine P3HT:$PC_{60}BM$ blend film without $N(BAI)_3$ (0 wt% in **Figure 3a**), the addition of 1 wt% $N(BAI)_3$ resulted in clear nanoscale phase separation (**Figure 3b**). While the phase separation is clearly discernible in the 5 wt% blended film (**Figure 3c**), using a high percentage of $N(BAI)_3$ (10 wt%, **Figure 3d**) led to a smeared phase morphology. The improved phase separation may be attributed to the enhanced π-π stacking of P3HT molecules induced by the $N(BAI)_3$ mediator that possesses large π conjugation surface and good coplanarity. However, excess $N(BAI)_3$ molecules may interfere with P3HT aggregation and is thus detrimental to the formation of nanoscale donor-acceptor interfaces.

To probe the morphological changes caused by the $N(BAI)_3$ mediator, the P3HT:$PC_{60}BM$:$N(BAI)_3$ three-component thin films were characterized by GIWAXS to

reveal lateral crystalline domain information within the films (**Figure 4**). In the P3HT:$PC_{60}BM$ blend film without $N(BAI)_3$, the (100), (200), (300) peaks in the q_z direction are indicative of lamellar stacking of P3HT chains, while the (010) peak in the q_x direction represents the aromatic π-π stacking of chains (**Figure 4a-d**). $PC_{60}BM$ shows an isotropic orientation with a broad distribution of intensity in all directions, indicative of randomly oriented aggregates of the fullerene derivative. The vertical and lateral line profiles are shown in **Figure 4e** and **Figure 4f**, respectively. Introduction of 1 wt% $N(BAI)_3$ resulted in narrower lamellar stacking (100) peak and π-π stacking (010) peak, which means that the crystallites of P3HT are largest and perhaps more ordered when 1 wt% $N(BAI)_3$ is introduced, with lamellar and π-π stacking Scherrer sizes of 65.9 and 16.8 nm, respectively (**Table S3**). The azimuthal spread of the (100) and (010) peaks are also the narrowest for 1wt% blended film, suggesting the formation of more oriented polymer lamella. Crystallite sizes, and perhaps degree of order, decrease for all other weight ratios of $N(BAI)_3$ (including the neat blend), which agrees well with the observations from both absorption/PL spectra and AFM characterizations. It is hypothesized that at low blending ratio such as 1 wt%, $N(BAI)_3$ molecules are more evenly distributed in the active layer, and its interaction with active materials is conducive to nanoscale crystallization. As the percentage of $N(BAI)_3$ increases over 1 wt%, self-aggregation of $N(BAI)_3$ becomes more dominant, making it less desirable for nanoscale crystallization and phase separation.

In order to understand the impact of $N(BAI)_3$ mediator on the vertical phase morphology of the blended films, neutron reflectometry was employed as a complementary technique to GIWAXS. The neutron reflectivity curves for the

P3HT:$PC_{60}BM$ films blended with different amount of $N(BAI)_3$ mediator are shown in **Figure 5a**, from which the volume fraction profiles of $PC_{60}BM$ were obtained (**Figure 5b**) by fitting the neutron reflectivity profiles in **Figure 5a** with a previously established model.[27] The scattering length density model used to fit the neutron reflectivity profiles was shown in **Figure S5**. The comparison indicates that while the $PC_{60}BM$ fraction was rather evenly distributed across the depth of the thin films from the bottom substrate, clear contrasts were observed near the top interface of these films. The curve of the 1 wt% $N(BAI)_3$ blended thin film indicated the formation of a very thin $PC_{60}BM$ enriched layer residing at the interface between the active layer and the cathode (**Figure 5b**). The 5 wt% $N(BAI)_3$ blended thin film showed similar vertical morphology as the 1 wt% $N(BAI)_3$ film. The 0 and 10 wt% $N(BAI)_3$ films have similar vertical morphologies, suggesting that adding a larger amount of $N(BAI)_3$ does not improve the phase morphology. Furthermore, the surface roughness of P3HT: $PC_{60}BM$ films was reduced by adding 1 wt% $N(BAI)_3$, but increased when adding more $N(BAI)_3$, which is consistent with the observation from AFM height images (**Figure S6**). The reduction of surface roughness is attributed to the formation of a $PC_{60}BM$ thin layer on the surface of the blend films, an observation that is similar to solvent additive mediated extrusion of $PC_{60}BM$ molecules to the surface. It suggests that, when only a small amount (*i.e.* 1 wt%) of $N(BAI)_3$ is present, the interaction between the three components is balanced such that different vertical domains of $PC_{60}BM$ are formed to give a very thin interfacial layer at the surface of the blend film. Such a layer at the cathode/active layer interface in an OPV device can act as a hole-blocking layer and effectively reduce the charge recombination.

3. Conclusion

We have found that the PCE of prototypical P3HT:$PC_{60}BM$ solar cells can be enhanced by ~11% when adding only 1 wt% $N(BAI)_3$ into the active layer. The PCE enhancement is ascribed to two factors: one is the improvement of phase morphology of the active layer by the $N(BAI)_3$ mediator, which not only tunes molecular packing behavior for more ordered lamellar stacking (100) and aromatic (π-π) stacking (010), but also promotes the formation of thin layer of $PC_{60}BM$ at the cathode/active layer interface to reduce the charge recombination; the other is the additional optical absorption by the $N(BAI)_3$ mediator which also contributes to the photocurrent generation for higher PCEs. The use of $N(BAI)_3$ as a solid-state photoactive mediator serves as a proof-of-principle that blending is a promising alternative to the commonly used solvent additives to improve the performance of OPVs or other optoelectronic devices. It is envisioned that the solid-state photoactive molecular mediator $N(BAI)_3$ may yield more stable device performance compared to the commonly used liquid-state processing additives due to the absence of slow evaporation or migration of solvent additive residues in the bulk heterojunction films. In addition, it has been shown that multi-armed molecules can facilitate the formation of a locked 3D mesh of donor polymer matrix through strong charge transfer interactions, resulting in enhanced thermal stability of devices by impeding the diffusion and aggregation of embedded $PC_{60}BM$ molecules.[28] More comprehensive studies towards nanophase stability of the active layer and device stability are ongoing in our lab.

4. Experimental Section

Device fabrication: The PEDOT:PSS was spun cast on clean ITO glasses at 4000 rpm for 60 seconds, followed by a thermal annealing at 135 ^{o}C for 20 min. The

P3HT:$PC_{60}BM$ mixture (weight ratio 1: 1) was dissolved in dichlorobenzene (DCB) to form a solution with a concentration of 40 mg/mL. The P3HT:$PC_{60}BM$ solution was then blended with different weight percentage of $N(BAI)_3$ (0 wt%, 1 wt%, 5 wt%, and 10 wt%). The $N(BAI)_3$ was dissolved in chloroform at a concentration of 20 mg/mL. The final concentration of the mixture solution was 35 mg/mL. After thermal annealing at 110 ^oC for 10 min. in the glovebox, 20 nm-thick calcium and 100 nm-thick aluminum layers were subsequently deposited on the active films under vacuum condition of 2×10^{-6} mbar. The device area was ~3 mm^2.

Thin films and device characterization: *J-V* curves were measured in the N_2 environment under illumination of 100 mW/cm^2 (1 sun, AM 1.5 G), which was calibrated with a standard Newport silicon diode. EQEs were acquired with a home-built system. Photoluminescence spectra were collected using a Horiba NanoLog Spectrofluorometer with an excitation wavelength of 500 nm. The absorption spectra were obtained from a Cary 5000 UV-Vis-NIR spectrometer. All the film samples were prepared on quartz glasses. AFM images were acquired with an Asylum MFP-3D Stand Alone AFM from Oxford Instruments, using tapping mode in air under ambient conditions. GIWAXS measurements were conducted at Beamline 7.3.3 at Advanced Light Source of the Lawrence Berkeley with X-ray energy of 10 keV, and the incident angle of X-rays was 0.15^o. Neutron reflectometry measurements were carried out at the Liquids Reflectometer (Beamline-4B) of Spallation Neutron Source (SNS), Oak Ridge National Laboratory (ORNL).

Supporting Information

Supporting Information is available from the Wiley Online Library or from the author.

Acknowledgements

This work was performed at the Molecular Foundry, and the X-ray experiments were conducted at the Advanced Light Source (ALS), Lawrence Berkeley National Laboratory, all supported by the Office of Science, Office of Basic Energy Sciences, of the U. S. Department of Energy under Contract No. DE-AC02-05CH11231. J. K. K. and J. F. B. acknowledge the financial support of Spallation Neutron Source (SNS), Oak Ridge National Laboratory (ORNL), which is sponsored by the ORNL Scientific User Facilities Division and DOE Office of Basic Research Sciences. B. Y. and M. K. contributed equally to this work.

Received: ((will be filled in by the editorial staff))
Revised: ((will be filled in by the editorial staff))
Published online: ((will be filled in by the editorial staff))

References

[1] a) A. J. Heeger, *Adv. Mater.* **2014**, *26*, 10; b) F. C. Krebs, N. Espinosa, M. Hösel, R. R. Søndergaard, M. Jørgensen, *Adv. Mater.* **2014**, *26*, 29.
[2] G. Li, V. Shrotriya, J. Huang, Y. Yao, T. Moriarty, K. Emery, Y. Yang, *Nat. Mater.* **2005**, *4*, 864.
[3] a) V. Shrotriya, *Nat. Photon.* **2009**, *3*, 447; b) S. Berny, N. Blouin, A. Distler, H. J. Egelhaaf, M. Krompiec, A. Lohr, O. R. Lozman, G. E. Morse, L. Nanson, A. Pron, *Adv. Sci.* **2016**, *3*, 1500342; c) Z. Ding, V. Stoichkov, M. Horie, E. Brousseau, J. Kettle, *Sol. Energ. Mat. Sol. Cells* **2016**, *157*, 305; d) S.-H. Bae, H. Zhao, Y.-T. Hsieh, L. Zuo, N. De Marco, Y. S. Rim, G. Li, Y. Yang, *Chem* **2016**, *1*, 197.

[4] B. Yang, M. Shao, J. Keum, D. Geohegan, K. Xiao, in *Semiconductor Materials for Solar Photovoltaic Cells*, Springer, 2016, 197.
[5] a) M. Li, K. Gao, X. Wan, Q. Zhang, B. Kan, R. Xia, F. Liu, X. Yang, H. Feng, W. Ni, *Nat. Photon.* **2017**, *11*, 85; b) W. Zhao, S. Li, H. Yao, S. Zhang, Y. Zhang, B. Yang, J. Hou, *J. Am. Chem. Soc.* **2017**, *139*, 7148; c) Y. Cui, H. Yao, B. Gao, Y. Qin, S. Zhang, B. Yang, C. He, B. Xu, J. Hou, *J. Am. Chem. Soc.* **2017**, *139*, 7302; d) W. Chen, Q. Zhang, *J. Mater. Chem. C* **2017**, *5*, 1275.
[6] a) P. W. M. Blom, V. D. Mihailetchi, L. J. A. Koster, D. E. Markov, *Adv. Mater.* **2007**, *19*, 1551; b) K.-H. Kim, H. Kang, H. J. Kim, P. S. Kim, S. C. Yoon, B. J. Kim, *Chem. Mater.* **2012**, *24*, 2373.
[7] a) S. J. Lou, J. M. Szarko, T. Xu, L. Yu, T. J. Marks, L. X. Chen, *J. Am. Chem. Soc.* **2011**, *133*, 20661; b) M. Shao, J. K. Keum, R. Kumar, J. Chen, J. F. Browning, S. Das, W. Chen, J. Hou, C. Do, K. C. Littrell, *Adv. Funct. Mater.* **2014**, *24*, 6647.
[8] a) A. M. Poe, A. M. Della Pelle, A. V. Subrahmanyam, W. White, G. Wantz, S. Thayumanavan, *Chem. Commun.* **2014**, *50*, 2913; b) Q. V. Hoang, S. Rasool, S. Oh, D. Van Vu, D. H. Kim, H. K. Lee, C. E. Song, S. K. Lee, J.-C. Lee, S.-J. Moon, *J. Mater. Chem. C* **2017** *5*, 7837; c) N. Shin, L. J. Richter, A. A. Herzing, R. J. Kline, D. M. DeLongchamp, *Adv. Energy Mater.* **2013**, *3*, 938.
[9] a) C. H. Y. Ho, Q. Dong, H. Yin, W. W. K. Leung, Q. Yang, H. K. H. Lee, S. W. Tsang, S. K. So, *Adv. Mater. Interfaces* **2015**, *2*; b) L. A. Perez, J. T. Rogers, M. A. Brady, Y. Sun, G. C. Welch, K. Schmidt, M. F. Toney, H. Jinnai, A. J. Heeger, M. L. Chabinyc, *Chem. Mater.* **2014**, *26*, 6531; c) J. Kniepert, I. Lange, J. Heidbrink, J. Kurpiers, T. J. Brenner, L. J. A. Koster, D. Neher, *J. Phys. Chem. C* **2015**, *119*, 8310.
[10] Z. Xiao, Y. Yuan, B. Yang, J. VanDerslice, J. Chen, O. Dyck, G. Duscher, J. Huang, *Adv. Mater.* **2014**, *26*, 3068.
[11] a) H. Cho, S.-H. Jeong, M.-H. Park, Y.-H. Kim, C. Wolf, C.-L. Lee, J. H. Heo, A. Sadhanala, N. Myoung, S. Yoo, *Science* **2015**, *350*, 1222; b) H. Waters, N. Bristow, O. Moudam, S.-W. Chang, C.-J. Su, W.-R. Wu, U.-S. Jeng, M. Horie, J. Kettle, *Org. Electron.* **2014**, *15*, 2433.
[12] a) B. J. Tremolet de Villers, K. A. O'Hara, D. P. Ostrowski, P. H. Biddle, S. E. Shaheen, M. L. Chabinyc, D. C. Olson, N. Kopidakis, *Chem. Mater.* **2016**, *28*, 876; b) P. Cheng, X. Zhan, *Chem. Soc. Rev.* **2016**, *45*, 2544.
[13] C. J. Schaffer, C. M. Palumbiny, M. A. Niedermeier, C. Burger, G. Santoro, S. V. Roth, P. Müller‐Buschbaum, *Adv. Energy Mater.* **2016**, *6*, 1600712
[14] a) Y. S. Chung, N. Shin, J. Kang, Y. Jo, V. M. Prabhu, S. K. Satija, R. J. Kline, D. M. Delongchamp, M. F. Toney, M. A. Loth, B. Purushothaman, J. E. Anthony, D. Y. Yoon, *J. Am. Chem. Soc.* **2011**, *133*, 412; b) J. Smith, W. Zhang, R. Sougrat, K. Zhao, R. Li, D. Cha, A. Amassian, M. Heeney, I. Mcculloch, T. D. Anthopoulos, *Adv. Mater.* **2012**, *24*, 2441; c) Z. Wei, H. Xi, H. Dong, L. Wang, W. Xu, W. Hu, D. Zhu, *J. Mater. Chem.* **2010**, *20*, 1203; d) Y. Zhang, D. Hanifi, E. Lim, S. Chourou, S. Alvarez, A. Pun, A. Hexemer, B. Ma, Y. Liu, *Adv. Mater.* **2014**, *26*, 1223.

[15] a) K. H. Park, Y. An, S. Jung, H. Park, C. Yang, *Energy Environ. Sci.* **2016**, *9*, 3464; b) K. R. M. J. S. R. S. J. W. C. H. S. F. S. F. K. B. R. J. R. Graham, *ACS Appl. Mater. Interfaces* **2011**, *3*, 1210.
[16] J. Wang, K. Liu, L. Ma, X. Zhan, *Chem. Rev.* **2016**, *116*, 14675.
[17] D. Sahu, C.-H. Tsai, H.-Y. Wei, K.-C. Ho, F.-C. Chang, C.-W. Chu, *J. Mater. Chem.* **2012**, *22*, 7945.
[18] E. Busseron, J.-J. Cid, A. Wolf, G. Du, E. Moulin, G. Fuks, M. Maaloum, P. Polavarapu, A. Ruff, A.-K. Saur, S. Ludwigs, N. Giuseppone, *ACS Nano* **2015**, *9*, 2760.
[19] B. He, A. B. Pun, D. Zherebetskyy, Y. Liu, F. Liu, L. M. Klivansky, A. M. McGough, B. A. Zhang, K. Lo, T. P. Russell, *J. Am. Chem. Soc.* **2014**, *136*, 15093.
[20] M. A. Kolaczkowski, B. He, Y. Liu, *Org. Lett.* **2016**, *18*, 5224.
[21] a) B. He, W. T. Neo, T. L. Chen, L. M. Klivansky, H. Wang, T. Tan, S. J. Teat, J. Xu, Y. Liu, *ACS Sustainable Chem. Eng.* **2016**, *4*, 2797; b) B. Z. He, D.; Wang, H.; Kolaczkowski, M. A.; Klivansky, L. M.; Tan, T.; Wang, L.; Liu, Y, *Chem. Sci.* **2016**, *7*, 3857; c) A. Osherov, E. M. Hutter, K. Galkowski, R. Brenes, D. K. Maude, R. J. Nicholas, P. Plochocka, V. Bulović, T. J. Savenije, S. D. Stranks, *Adv. Mater.* **2016**, *28*, 10757.
[22] S. Gunes, Neugebauer, H. Sariciftci, N. S. , *Chem. Rev.* **2007**, *107*, 1324.
[23] B. Yang, Y. Yuan, J. Huang, *J. Phys. Chem. C* **2014**, *118*, 5196.
[24] K. Yuan, L. Chen, Y. Chen, *J. Mater. Chem. C* **2014**, *2*, 3835.
[25] a) H. Yamagata, F. C. Spano, *J. Chem. Phys.* **2012**, *136*, 184901; b) G. Nagarjuna, M. Baghgar, J. A. Labastide, D. D. Algaier, M. D. Barnes, D. Venkataraman, *ACS Nano* **2012**, *6*, 10750.
[26] a) B. Yang, Y. Yuan, P. Sharma, S. Poddar, R. Korlacki, S. Ducharme, A. Gruverman, R. Saraf, J. Huang, *Adv. Mater.* **2012**, *24*, 1455; b) Z. Ye, X. Zhao, *J. Microsc.* **2010**, *238*, 27.
[27] a) M. Shao, J. Keum, J. Chen, Y. He, W. Chen, J. F. Browning, J. Jakowski, B. G. Sumpter, I. N. Ivanov, Y.-Z. Ma, C. M. Rouleau, S. C. Smith, D. B. Geohegan, K. Hong, K. Xiao, *Nat. Commun.* **2014**, *5*, 3180; b) J. K. B. Keum, J.F.; Xiao, K.; Shao, M.; Halbert, C.E.; Hong, K., *Appl. Phys. Lett.* **2013**, *103*, 223301.
[28] C. H. Yi Ho, H. Cao, Y. Lu, T.-K. Lau, S. H. Cheung, H.-W. Li, H. Yin, K. L. Chiu, L.-K. Ma, Y. Cheng, S.-W. Tsang, X. Lu, S. K. So, B. S. Ong, *J. Mater. Chem. A* **2017**, *5*, 23662.

Figures

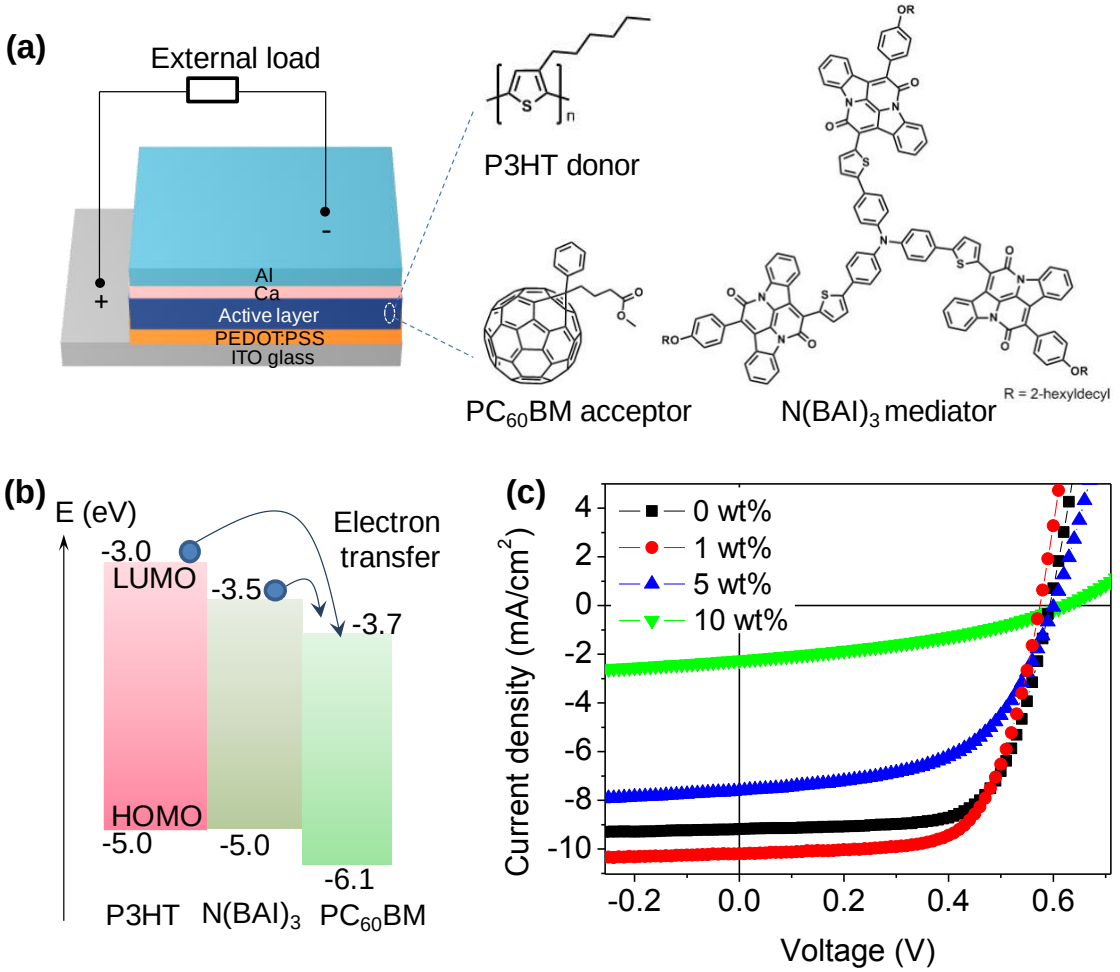

Figure 1. (a) The device structure (ITO/PEDOT:PSS/P3HT:$PC_{60}BM$:$N(BAI)_3$/Ca/Al) and molecular structures of P3HT, $PC_{60}BM$ and $N(BAI)_3$. (b) The energy diagram of the P3HT:$PC_{60}BM$:$N(BAI)_3$ ternary devices to show charge flow. (c) *J*-*V* curves obtained from devices with different weight percentage (black: 0 wt%, red: 1 wt%, blue: 5 wt%, green: 10 wt%) of $N(BAI)_3$ in the P3HT:$PC_{60}BM$ blend film under illumination of 100 mW/cm^2 (1 sun, AM 1.5 G)

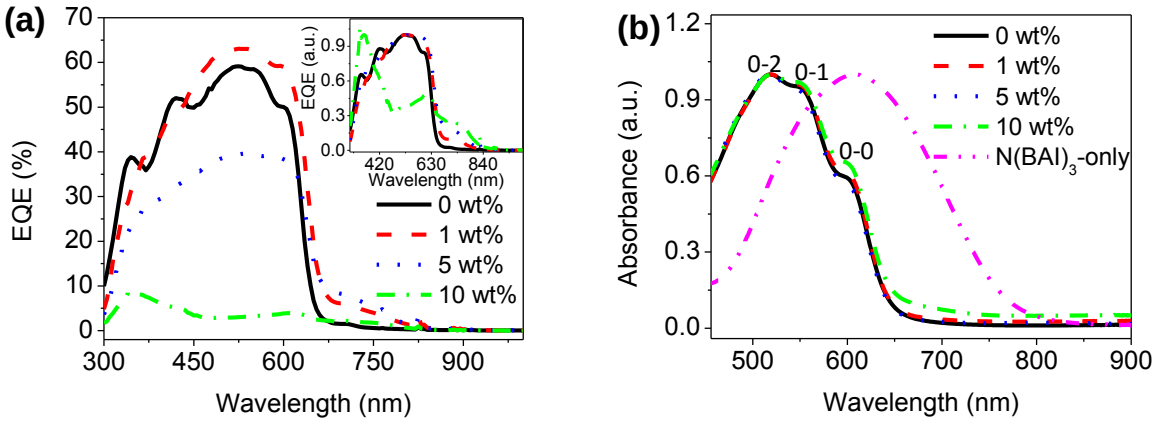

Figure 2. (a) External quantum efficiencies (EQEs) obtained from devices with different weight percentage (black: 0 wt%, red: 1 wt%, blue: 5 wt%, green: 10 wt%) of $N(BAI)_3$ in the P3HT:$PC_{60}BM$ blend films, and the inset showing the normalized EQE curves, which were normalized to the highest EQE of each curve. (b) Absorption spectra of the P3HT-only film, P3HT films blended with different $N(BAI)_3$ ratio, and $N(BAI)_3$-only film, in which 0-2, 0-1, and 0-0 vibronic transitions from the ground state to the excited states are labeled.

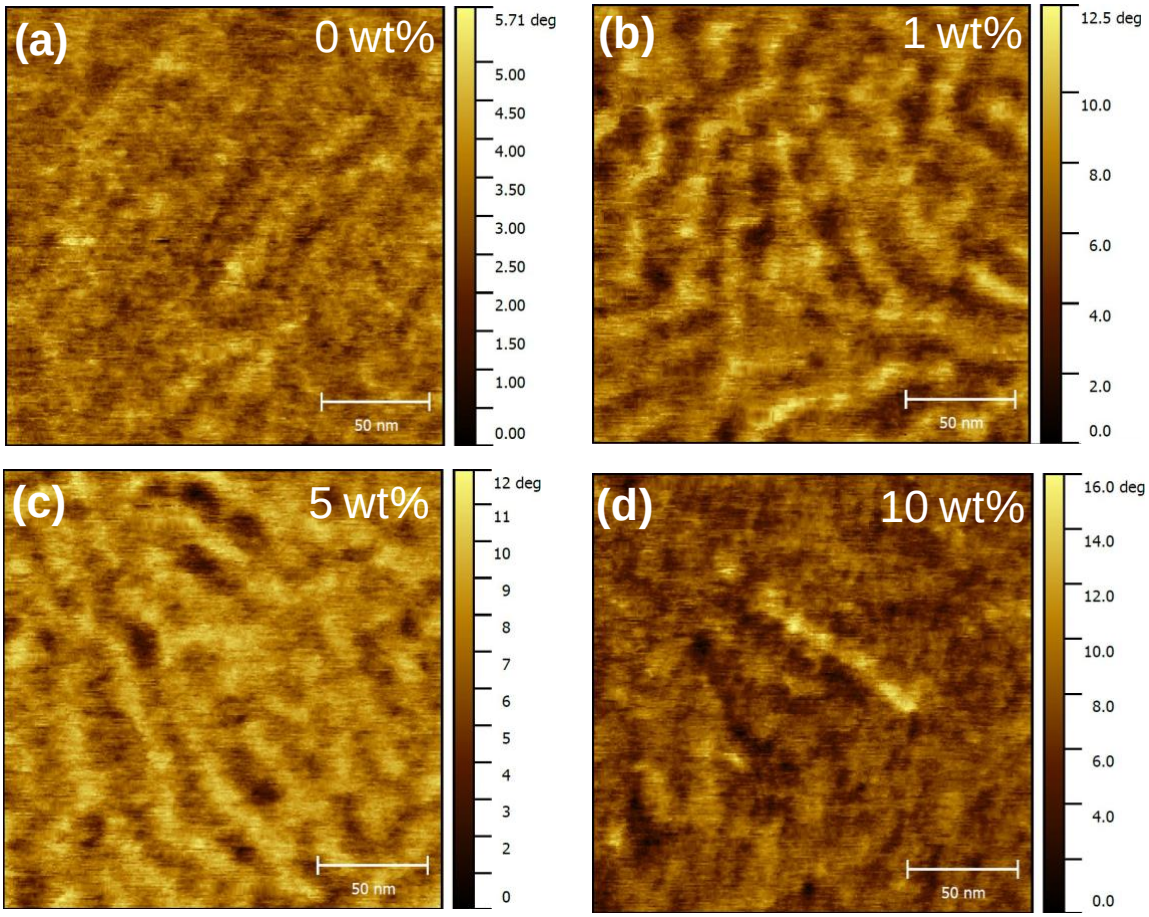

Figure 3. AFM phase image obtained from P3HT:$PC_{60}BM$ films blended with different weight percentage of $N(BAI)_3$: (a) 0 wt%, (b) 1 wt%, (c) 5 wt%, and (d) 10 wt%.

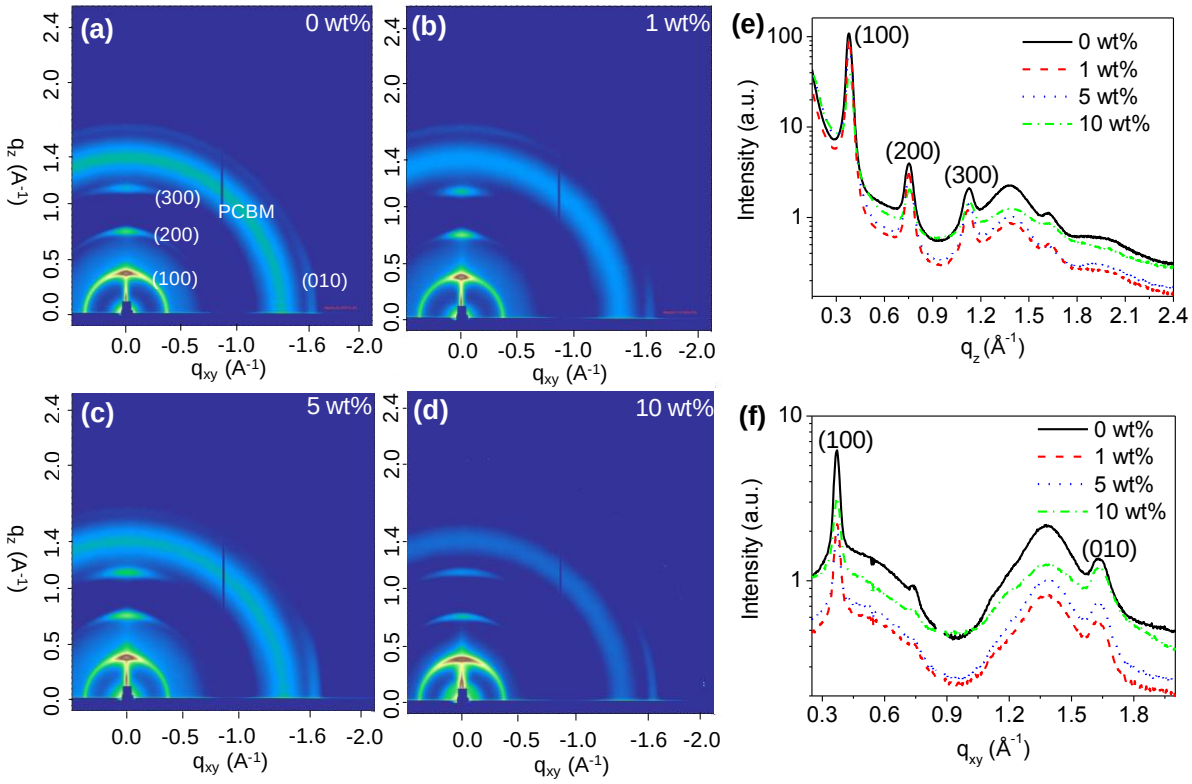

Figure 4. GIWAXS patterns obtained from P3HT:$PC_{60}BM$ films blended with different weight percentage of $N(BAI)_3$: (a) 0 wt%, (b) 1 wt%, (c) 5 wt%, and (d) 10 wt%; (e) and (f) show **t**he corresponding vertical and lateral line profiles, respectively.

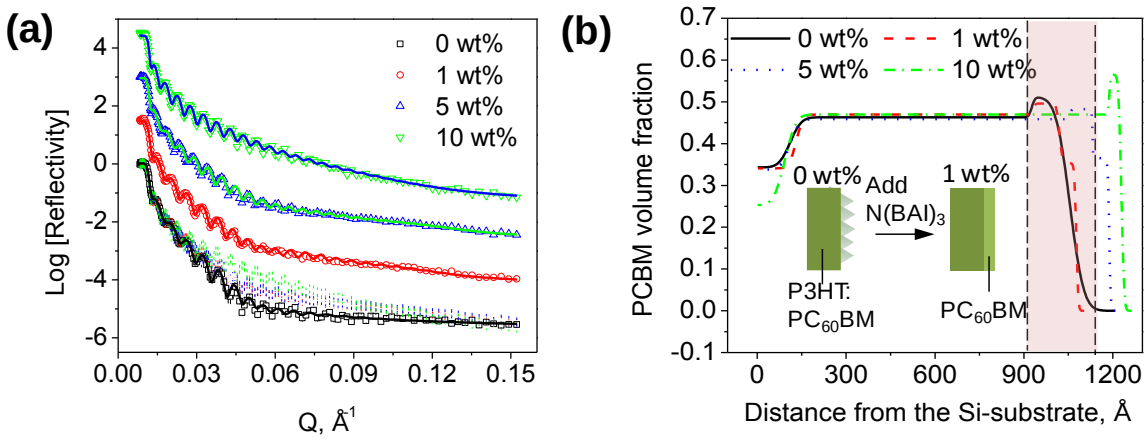

Figure 5. (a) Neutron reflectivity curves for different percentage (black: 0 wt%, red: 1 wt%, blue: 5 wt%, green: 10 wt%) of $N(BAI)_3$ in the P3HT:$PC_{60}BM$ films; (b) Volume fraction profiles for four different percentage of $N(BAI)_3$ mediators, and the inset of a schematic diagram showing that the film roughness is reduced while a thin layer of $PC_{60}BM$ forms by adding 1 wt% $N(BAI)_3$. The volume fraction profiles were deduced from the data fits of the neutron reflectivity profiles shown in (a) as established in reference 27

Enhancing the Efficiency of Organic Photovoltaics by a Photoactive Molecular Mediator

*Bin Yang, Matthew A. Kolaczkowski, Michael A. Brady, Jong K. Keum, James F. Browning, Teresa L. Chen, Yi Liu**

A solid-state photoactive molecular mediator $N(BAI)_3$ was developed as an alternative to the commonly used solvent processing additives to achieve 11% enhancement of power conversion efficiency of prototypical poly(3-hexylthiophene-2,5-diyl) (P3HT):$PC_{60}BM$ bulk heterojunction photovoltaic devices, attributable to both fine tuned phase morphology and addition optical absorption from the molecular additives.

Keywords: Conjugated molecular materials; Organic optoelectronics; Organic photovoltaics; Morphology

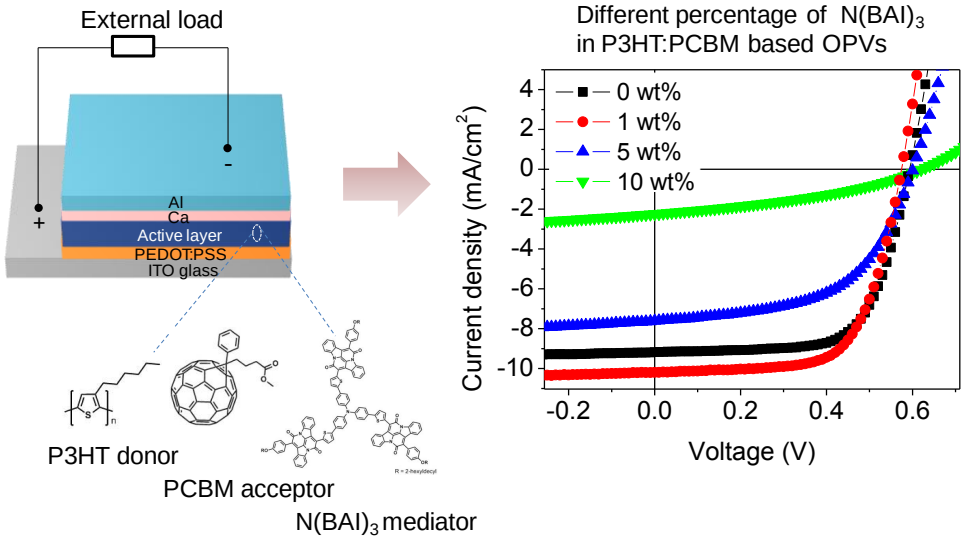
External load
-
+
Al
Ca
Active layer
PEDOT:PSS
ITO glass
P3HT donor
PCBM acceptor
N(BAI)3 mediator
Different percentage of N(BAI)3
in P3HT:PCBM based OPVs
0 wt%
1 wt%
5 wt%
10 wt%
Current density (mA/cm2)
Voltage (V)
4
2
0
-2
-4
-6
-8
-10
-0.2
0.0
0.2
0.4
0.6